ACS APPLIED MATERIALS & INTERFACES

www.acsami.org

Research Article

Ultrasensitive and Stretchable Conductive Fibers Using Percolated Pd Nanoparticle Networks for Multisensing Wearable Electronics: Crack-Based Strain and H_2 Sensors

Chihyeong Won, Sanggeun Lee, Han Hee Jung, Janghoon Woo, Kukro Yoon, Jaehong Lee, Chaebeen Kwon, Minkyu Lee, Heetak Han, Yongfeng Mei,* Kyung-In Jang,* and Taeyoon Lee*

Cite This: *ACS Appl. Mater. Interfaces* 2020, 12, 45243−45253

Read Online

ACCESS | Metrics & More | Article Recommendations | Supporting Information

ABSTRACT: The need for wearable electronic devices continues to grow, and the research is under way for stretchable fiber-type sensors that are sensitive to the surrounding atmosphere and will provide proficient measurement capabilities. Currently, one-dimensional fiber sensors have several limitations for their extensive use because of the complex structures of the sensing mechanisms. Thus, it is essential to miniaturize these materials with durability while integrating multiple sensing capabilities. Herein, we present an ultrasensitive and stretchable conductive fiber sensor using PdNP networks embedded in elastomeric polymers for crack-based strain and H_2 sensing. The fiber multimodal sensors show a gauge factor of ∼2040 under 70% strain and reliable mechanical deformation tolerance (10,000 stretching cycles) in the strain-sensor mode. For H_2 sensing, the fiber multimodal sensors exhibit a wide sensing range of high sensitivity: −0.43% response at 5 ppm (0.0005%) H_2 gas and −27.3% response at 10% H_2 gas. For the first time, we demonstrate highly stretchable H_2 sensors that can detect H_2 gas under 110% strain with mechanical durability. As demonstrated, their stable performance allows them to be used in wearable applications that integrate fiber multimodal sensors into industrial safety clothing along with a microinorganic light-emitting diode for visual indication, which exhibits proper activation upon H_2 gas exposure.

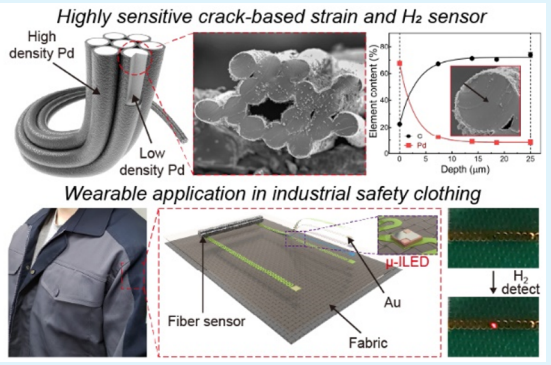

KEYWORDS: *fiber-type multimodal sensor, hydrogen sensors, strain sensors, stretchable electronics, wearable electronics*

Downloaded via FUDAN UNIV on October 15, 2020 at 03:39:35 (UTC).
See https://pubs.acs.org/sharingguidelines for options on how to legitimately share published articles.

INTRODUCTION

Wearable fiber-type electronic devices have low weight, flexibility, and conformable characteristics and have attracted increasing research attention.[1−3] Currently, researchers have focused on the miniaturization and versatility of the materials while maintaining mechanical reliability under various types of deformations (e.g., bending, distortion, and stretching). Current one-dimensional wearable device structures[4,5] require a combination of electrically conductive components and elastic fibrous matrices so that the devices will maintain essential flexibility and stretchability.[6] In terms of conductive materials, carbon nanotubes,[7,8] graphene,[9,10] hydrogels,[11,12] and metal-based nanoparticles (NPs)[13,14] or nanowires (NWs)[15,16] are used as conductive networks in these flexible matrices. Moreover, electrodes comprising metal nanostructures embedded in polymer matrices have high stretchability while maintaining key electrical properties.[6]

Owing to its low resistivity, high ductility, and malleability, Pd is a metal that is widely used in catalysts,[17−19] H_2 storage devices,[20−22] and other electronic devices.[23−29] It also has excellent H_2 absorption capacity compared to other metals. In particular, Pd has a metal-lattice volume expansion property when compounded with H_2 molecules.[30] PdHx compounds formed by the combination of Pd and H_2 molecules have low electrical conductivity compared with Pd particles alone.[31] In this regard, flexible H_2 sensors using Pd can be developed by combining the characteristics of particle-to-particle distance control and by changing particle conductivity. Furthermore, research studies related to combining Pd nanostructures by inducing mechanical strain significantly enhance their sensor sensitivity with elasticity.[32−35] Noh and co-workers demonstrated a flexible H_2 sensor with nanogaps in a Pd thin film by sputtering on a prestretched poly(dimethylsiloxane) (PDMS) substrate.[36] In this research, Pd nanocracks were generated by stretching and releasing of Pd/PDMS to investigate the gas-detection properties of elastic devices. Kim et al. proposed flexible H_2-sensing platforms using yarn spun polyacrylonitrile

Received: June 8, 2020
Accepted: September 7, 2020
Published: September 7, 2020

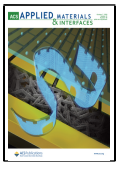

© 2020 American Chemical Society

https://dx.doi.org/10.1021/acsami.0c10460
ACS Appl. Mater. Interfaces 2020, 12, 45243−45253

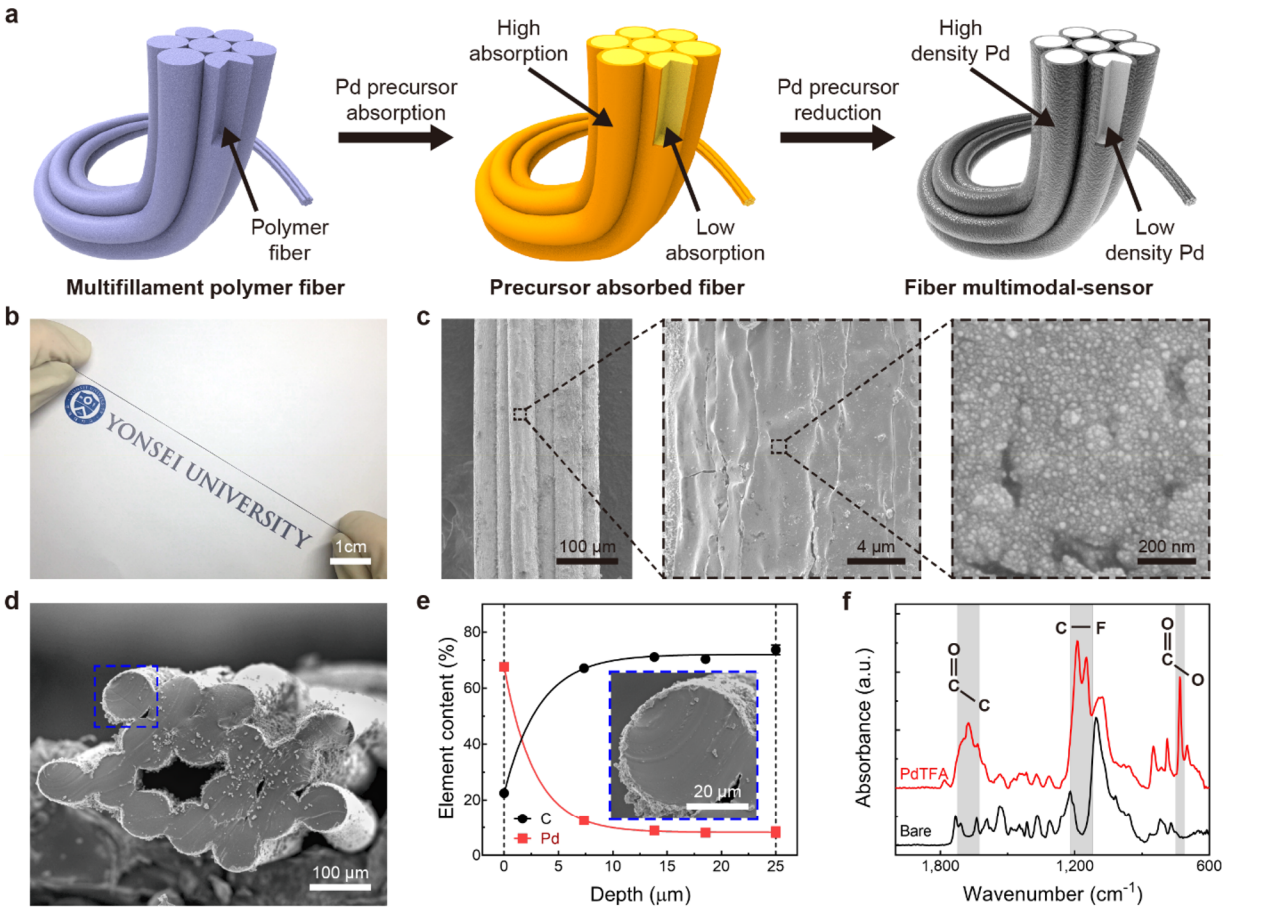

Figure 1. (a) Schematic of the fabrication process of the fiber multimodal sensor. (b) Photograph of a 50% strained fiber multimodal sensor. (c) SEM image of the fiber. (d) Cross-sectional SEM image of the fiber. (e) EDS analysis of a single fiber filament. (f) FTIR analysis of a bare fiber and a PdTFA swollen fiber.

(PAN) polymer nanofiber-coated Pd layers and thin-over-layered Pt.[37] The simply fabricated sensors were flexible and free-standing single-strand yarn scaffolds having nanograined Pd and nanogaps. However, since the Pd-sensing materials were deposited onto elastic substrates, the mechanical stability was inadequate, and the H_2 sensors were not stretchable enough. In addition, flexible sensors that simultaneously detect H_2 and measure mechanical deformation using Pd have been under-researched, despite the urgency that we integrate stretchable fiber H_2 sensors that are easily elongated into textiles and clothes for the real-time detection of H_2 gas.

In this research, we propose a sensitive and stretchable conductive fiber sensor using PdNP networks embedded in elastomeric polymers for crack-based multisensors[38,39] that strain and H_2 gas sensing. A simple two-step chemical solution process is used to fabricate the sensor at room temperature, resulting in a polyurethane (PU) fiber embedded with PdNPs. The fiber multimodal strain sensor shows a gauge factor (GF) of ~2040 under 70% strain and reliable mechanical deformation tolerance (10,000 stretching cycles). As a gas sensor, the fiber detects H_2 gas by measuring the change in the electrical resistance of the PdNPs in the fiber without interconnecting other devices. The developed fiber sensor exhibits high response to electrical resistance (−27.3%) at 10% H_2 gas, a wide range detection of 5 ppm (0.0005%) to 10% H_2 at room temperature, and response and recovery times of 30 s each. In terms of the simultaneous sensing of stretching and gas-sensing properties, the sensing range of the H_2 gas response was remarkably maintained under the conditions of up to 110% strain. To demonstrate the H_2 gas-sensitive fiber, we integrate a fiber multimodal sensor and a microinorganic light emitting diode (μ-ILED) device as a visualized indicator to warn a human wearer about H_2 gas leakage and to show its great application potential as a smart safety device.

RESULTS AND DISCUSSION

Fabrication of Multimodal Fiber Sensors Using a Simple Solution Process. Figure 1a illustrates the fabrication process of the highly sensitive and stretchable conductive fiber multimodal sensor. To fabricate highly sensitive fiber sensors, it is essential to absorb the Pd precursor into stretchable fibers and to reduce the absorbed Pd precursor into PdNPs to form the connecting network in the fibers. A commercial multifilament PU fiber was immersed in a 20 wt % Pd trifluoroacetate (PdTFA) solution in isopropyl alcohol (IPA) for 30 min. Trifluoroacetate anion (CF_3COO^-)-based metal precursors were used for silver-based conductive fibers, owing to the resulting ion−dipole interaction with the hydroxyl groups (−OH) of the alcoholic solvent that leads to higher efficiency.[14] The fiber was then dried in air for 10 min followed by immersing in diluted hydrazine hydrate ($N_2H_4 \cdot xH_2O$) as a reducing agent. After 10 min, the fiber was rinsed in deionized water and dried again in air. Using this fabrication procedure, the Pd precursor was highly absorbed onto the surface of the fiber, which resulted in high-density PdNP

https://dx.doi.org/10.1021/acsami.0c10460
ACS Appl. Mater. Interfaces 2020, 12, 45243−45253

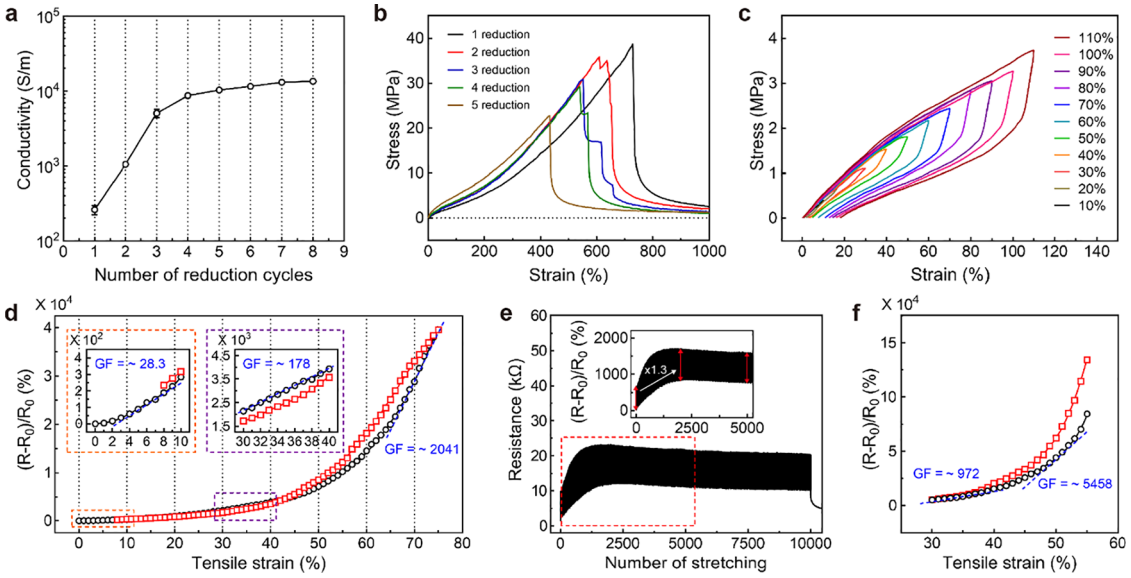

Figure 2. (a) Electrical conductivity of the fiber multimodal sensor according to the cycles of the solution process of Pd ions. (b) Stress−strain curve of the fiber multimodal sensor fabricated with 1−5 solution-process cycles of Pd ions. (c) Stress−strain curves of the fiber multimodal sensor for 0−110% strains, showing mechanical hysteresis according to the strains of the fiber. (d) Relative change in the electrical resistance of the fiber for tensile strain. The inset graphs show the relative changes in the electrical resistance of the fiber for strain within the range of 0−10 and 30−40%, respectively. (e) Electrical resistance of the fiber multimodal sensor to the repeated strains of 10% during 10,000 cycles. The inset graph shows the range of stretching numbers between 0 and 5000. (f) Relative change in the electrical resistance of the fiber after sufficient stretching cycles.

formation on the surface. Figure 1b displays a photograph of a 50%-strained fiber multimodal sensor. The original color of the PU fiber (white) turned black because of the reduction process of the Pd precursor into PdNPs (Figure S1), and the stretchability of fiber was maintained (Movie S1). Figure 1c shows typical scanning electron microscopy (SEM) images obtained from the fiber multimodal sensor without applying strain. This fiber sensor comprised multiple filaments whose diameter was approximately 35 μm. The magnified surface shows a smooth morphology comprising small PdNPs having an average size of approximately 20 nm, which agrees well with the estimated particle size of ~20.07 nm, found using the Scherrer equation via X-ray diffraction (XRD) (Figure S2). A cross-sectional SEM image of the multifilament fiber and its energy-dispersive X-ray spectroscopy (EDS) were measured to observe the distribution of PdNPs in the fiber, as shown in Figure 1d,e, respectively. The average component ratio of Pd in the fabricated fiber from the EDS analysis was 18.25%, which is consistent with the 17.4 wt % obtained via the thermogravimetric analysis (TGA) results (Figure S3). However, the Pd content on the shell was 67.6 wt % and abruptly decreased to 12.6 wt % at a 7.4 μm depth from the shell and to 8.9 wt % at 13.8 μm, as shown in Figure 1e. To confirm the sufficient absorption of the Pd precursor, Fourier-transform infrared spectroscopy (FTIR) measurements were conducted on the as-received PU fiber and the PdTFA-absorbed fiber. The results are presented in Figure 1f. The new peaks in the PdTFA-absorbed fiber were compared with the as-received PU fiber at 1147 and 1188 cm^{-1}, demonstrating that the asymmetric stretching vibrations of the C−F bonds in the Pd precursor represent the complete absorption of the Pd precursor into the fibers.[13] Different constituent proportions of Pd from the core and shell of the fiber were observed in the SEM image, differing from previous results that had a wider distribution of NPs throughout the fiber.[15,40] Because IPA was used as a solvent and according to the Hansen solubility parameter,[41] the PU fiber has a higher swelling ratio that leads to more abundant PdNPs on the shell than in the core.[42] The detailed data of the PdNP distribution are described in the Supporting Information.

Electrical and Mechanical Properties of Fiber Multimodal Sensors. PdNP-embedded stretchable fiber has different electrical and mechanical properties depending on the number of Pd precursor solution process cycles.[40] In Figure 2a, the initial conductivity of the fiber is 260.1 S/m, and as the number of reduction cycles increases, the conductivity of the fiber increases, owing to the formation of a PdNP shell on the outside of the fiber. When the number of reduction cycles exceeds four, the electrical conductivity path of the PdNP shell is maintained during the reduction process without increasing. Thus, the conductivity of the fiber converges at about 1.3×10^4 S/m. The mechanical rupture strain, as opposed to conductivity, tends to decrease as the number of reduction cycles increases (Figure 2b). The developed fiber should be able to withstand mechanical deformations in the 55% range induced by human movement.[43] As the PdNP that is formed inside the fiber increases with the number of reduction cycles, they break the elastomer connections and weaken the polymeric bonds in the fiber. However, the mechanical stretchability of the fiber is good enough to cover the strain-sensing range of the fiber strain sensor. When the fiber multimodal sensor is first stretched, cracks are generated in the PdNP shell, creating electrical and mechanical hysteresis properties during the first stretching and releasing cycle. As a result of measuring the mechanical hysteresis while increasing the strain from 10 to 110% of the fiber sensor fabricated via two solution-process cycles, the tendency of hysteresis appears constant, as shown in Figure 2c. Figure 2d shows the relative changes of the electrical resistance of the fiber multimodal sensor as a strain sensor. In the strain sensor mode, the fiber multimodal sensor shows a steep increase in electrical resistance with increasing strain and has a large GF in the

https://dx.doi.org/10.1021/acsami.0c10460
ACS Appl. Mater. Interfaces 2020, 12, 45243−45253

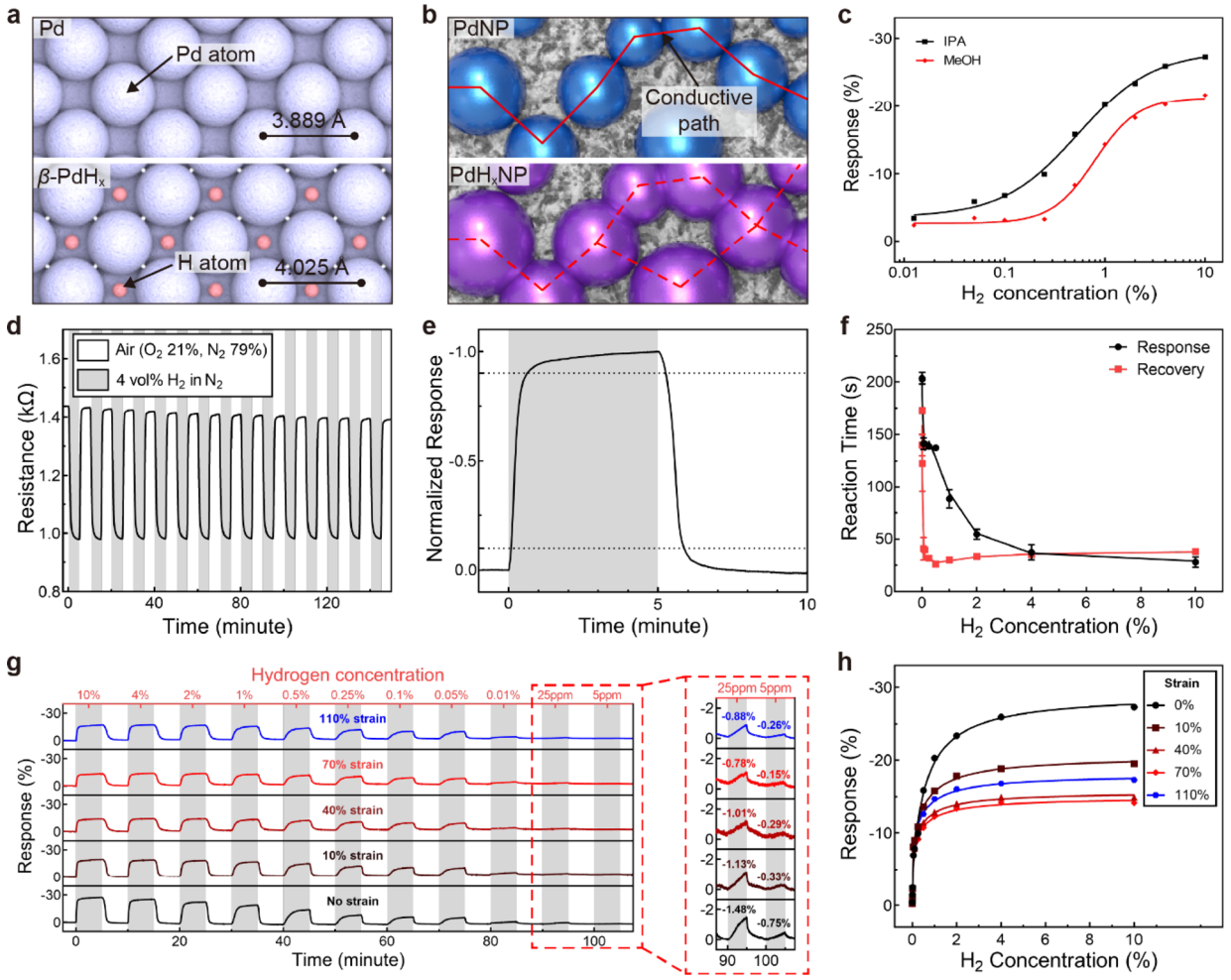

Figure 3. (a) Distance between Pd atoms in the original state and the Pd hydride state. (b) Structure of the conducting network regarding PdNPs and PdH_xNPs. (c) Responses of the fiber multimodal sensor fabricated by IPA and MeOH solvent. (d) Repeatability of the fiber multimodal sensor upon loading/unloading of 4% H_2. (e) Real-time behavior of a normalized reaction for 4% H_2 and air exposure showing response and recovery times. (f) Response and recovery times as functions of H_2 concentration. (g) Response of the 0−110% strained sensor for 10% to 5 ppm (0.0005%) H_2 gas. (h) Plots of sensor response for 0−110% strain as a function of H_2 concentration.

low strain range, because the resistance change is large, even with small strain changes. The GF of the strain sensor, obtained from the slope of the graph in Figure 2d, is generally defined as $GF = \delta((R - R_0)/R_0)/\delta\varepsilon$, where R and R_0 indicate the electrical resistance with and without tensile strain ε, respectively. The strain sensor exhibited a large GF of ∼2041 at a strain range within 65−75%, compared with a GF of ∼178 at a strain range within 30−40%, which is about 11 times different. This indicates that the tensile strain can be measured sensitively and precisely by the fiber strain sensor, even in a low-strain-sensing range. The response change during the stretching cycle shows that the difference in the electrical resistance change between stretching and releasing is negligible. During repeated stretching, more cracks are formed and electrical resistance increases continuously. Eventually, when the Pd cracks on the fiber surface converge via repeated stretching, the response via fiber strain increases even more. The conductive path of the fiber is much more susceptible to cracks in the outer PdNP shell of the fiber because PdNPs are formed more than 6 times on the inside of the fiber than on the outside. Figure 2e shows the electrical resistance measurement after stretching 10,000 cycles with a 10% strain. Initially, as the numbers of stretches increase, the difference between electrical resistances during stretching and releasing gradually increases. After 2000 stretching cycles, it shows a stable resistance difference. This indicates that the response of the same strain increases as the electrical resistance of the fiber increases until the crack formation in the PdNP shell converges. Then, the fiber acquires a stable operation. After convergence, we measured the electrical properties of the fiber strain (Figure 2f). The fiber multimodal sensor as a strain sensor showed a negligible hysteresis after repeated stretching. Thus, it has high elasticity and durability. The fiber after repeated stretching shows a significant GF of ∼972 at 30−40% strain range and a GF of ∼5458 at 45−55% strain. As the conductivity of the fiber is greatly influenced by the connection between the cracks of the Pd shells, the resistance change of the fiber due to strain becomes larger than before. This improves fiber strain sensor performance by more than 5 times at a low strain range, compared with the initial stretching cycle. Although the strain-sensing range has decreased, the sensor with numerous crack formations has high GF and is suitable for use as a H_2 sensor.

Characterization of H_2-Gas-Sensing Properties under Strain. To investigate the H_2-gas-sensing performance of the fiber multimodal sensor, the electrical properties of the

https://dx.doi.org/10.1021/acsami.0c10460
ACS Appl. Mater. Interfaces 2020, 12, 45243−45253

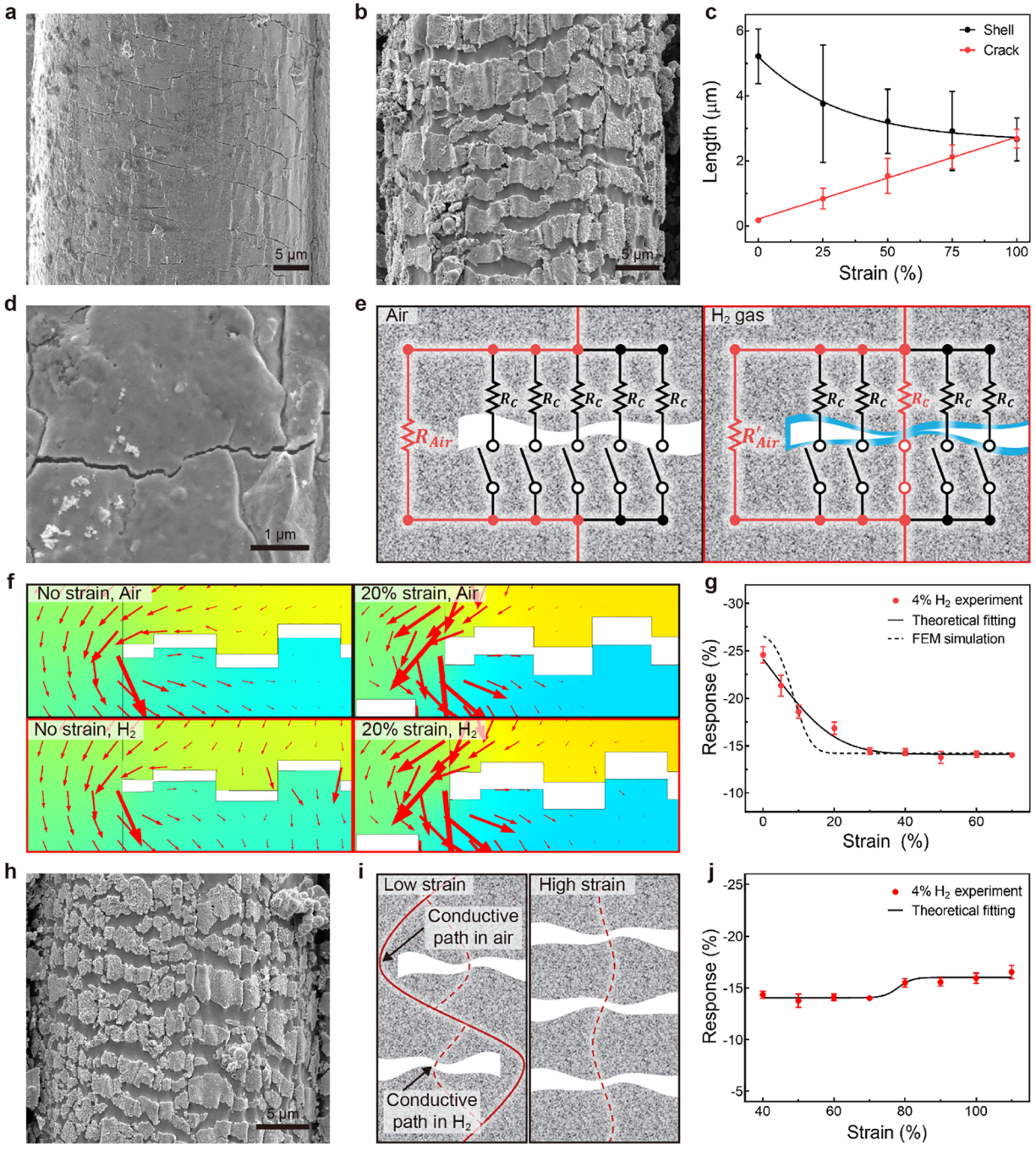

Figure 4. SEM image of a fiber multimodal sensor (a) exposed to H_2 gas and (b) under 50% strain after being exposed to H_2 gas. (c) PdNP/PU composite shell and crack length as a function of the applied strain. (d) SEM image of a crack showing nonuniform length. (e) Schematic showing a simplified circuitry model for the H_2 sensing mechanism. (f) FEM simulation of the current density for the shell at 0 and 20% strain in air and H_2. (g) 4% H_2 gas response of the fiber multimodal sensor up to 70% strains with theoretical fitting and FEM simulation results. (h) SEM image of a fiber multimodal sensor under 100% strain after exposure to H_2 gas. (i) Schematic of the crack structure and electrical paths in air and H_2 gas for low and high strain of fibers. (j) 4% H_2 gas response of the fiber multimodal sensor under 40−110% strains with the theoretical fitting.

fabricated fiber were analyzed according to many aspects. The dense PdNP network in the outer shell formed a conducting network that is closely related to H_2 gas sensitively. The conductivity of the PdNP/PU composite could thus be calculated using the 3D percolation theory as follows:

$$\sigma = \sigma_0(V_f - V_c)^s \quad (1)$$

where σ is the electrical conductivity of the PdNP/PU composite, σ_0 is the conductivity of the PdNP, V_f is the volume fraction of the PdNP, V_c is the volume fraction at the percolation threshold, and s is the critical exponent. In Figure 3a,b, pure Pd has a lattice constant of 3.889 Å. However, when it is exposed to H_2 gas, the H atoms are incorporated into the surface of the Pd layer, resulting in the formation of a semiconducting Pd hydride (β-PdH$_x$) having a lattice constant of 4.025 Å.[23] As the size of Pd particles increases, the connection of particles forms more conducting paths on the surface of the fiber, and the resistance lowers in terms of the

https://dx.doi.org/10.1021/acsami.0c10460
ACS Appl. Mater. Interfaces 2020, 12, 45243−45253

structure. However, PdH_x has a resistivity 1.9 times higher than that of pure Pd,[31] which leads to increased resistance, depending on the properties of Pd particles. This contradictory effect has a trade-off according to the Pd volume fraction. To maximize the resistance response of Pd when H_2 gas is applied, Pd particles should be formed more in the shell of the fiber than in the core to make it more sensitive. This hypothesis was directly confirmed by the SEM image of fibers, which compared alcoholic solvents used in the precursor solution (Figure 3c and Figure S4). The sensor response was defined as Response (%) $= \frac{R_{H_2} - R_{Air}}{R_{Air}}$, where R_{Air} and R_{H_2} are the resistances of the fiber before and after H_2 exposure, respectively. The fiber fabricated using an IPA solvent had a −27.3% response and that using a MeOH solvent had a 12.3% response (Figure S5). We have chosen IPA due to more stable and reproducible results under repeated mechanical strain, as opposed to the ones obtained when using samples where MeOH was employed. The calculation value of the H_2 gas response based on eq 1 and the interparticle distance model was about −27.0%: almost the same as the response value of the fiber sensor. A detailed calculation is shown in the Supporting Information.

To characterize H_2 gas sensing using a fiber multimodal sensor, we measured using an initial channel length of 2 cm inside a gas chamber. Figure 3d shows the response of a sample when exposed to air and 4% H_2 for 15 cycles. When the fiber was exposed to H_2, the resistance decreased and recovered under air with high reproducibility. Figure 3e shows the normalized response and recovery of a fiber exposed to 4% H_2 and recovered under air. Both the response and the recovery showed an initial fast reaction followed by slow relaxation. The response time is defined as the time required for the normalized resistance to change from −10 to −90% and vice versa for recovery time. The response time was 32.2 s, and the recovery time was 36.7 s in the given example. Figure 3f shows the response and recovery times when the H_2 concentration changes. Both response and recovery times increased at low H_2 concentrations. This can be explained by the reduced adsorption rate of H_2 on Pd at low H_2 concentrations according to the Langmuir adsorption isotherm.[44] The fiber showed a stable response and recovery time because of nanocracks in Pd shells. When the sample was strained at 0−110% strain, the base resistance increased but maintained a stable response. The samples were also exposed to a wide range of H_2 concentrations starting from 5 ppm (0.0005%) to 10%, as shown in Figure 3g. The sensor exhibited a wide detection range under no strain and the response of 10% and 5 ppm H_2 was approximately −27.3 and −0.75%, respectively. When the fiber was strained, some decrease was noticed in the response at 0−70% strain and a slight increase at 70−110% strain. However, a wide range of responses persisted (detailed analysis is presented in Figure 4). Figure 3h shows the calculated response values versus H_2 concentration for various strains (0, 10, 40, 70, and 110%). The sensor became gradually less sensitive up to 70% strain. However, the response of the sensor increases at 110% strain. The sensor response shows a rapid change at H_2 concentrations below a 2% range and shows a saturated response at H_2 concentrations over 4%. Also, the sensor could effectively detect H_2 gas leakage below its minimum flammable range, which is 4%.[45] It should be noted that the miscible gap generally found in Pd-based fiber sensors was not observed.[46] The miscible gap in the H_2 pressure−composition isotherm can be narrowed when PdNPs are used, owing to their large surface area,[47] which results in curves similar to other H_2 gas sensors that use networked nanoscale Pd.[48,49] The tensile strain applied to the fiber sensor under an H_2 environment can be readily compensated by additionally using the fiber strain sensors reported previously.[40]

Pd Crack-Based Multimodal Sensing Mechanism. The difference between the sensor response versus strain can be attributed to the geometrical effect. Figure 4a shows an SEM image for the fiber multimodal sensor after exposure to H_2. Some cracks were observed, although the fiber was not strained. Previous reports show that the expansion of Pd thin films can lead to crack generation caused by strain localization.[50] The volume of PdNPs increases when they are exposed to H_2, leading to an increase in PdNP/PU volume, which can generate cracks. Figure 4b shows an SEM image of a fiber strained at 50%, and Figure 4c shows the average length of shells and spacings between the cracked shells at different strains. As the fiber was strained, more and shorter PdNP shells were induced with longer cracks. Cracks were formed because of the different mechanical properties of the core and shell, resulting in the increase of electrical resistance.[40] Figure 4d shows an SEM image of a nanoscale crack generated on a fiber surface. It can be seen that the crack length is not uniform along the surface. This can result in partial crack connection under H_2 gas, owing to the shift of shells on elastomers, which can result in a few nanometer-sized cracks.[51] Based on this mechanism, the response was different when H_2 gas was applied to the strained fiber, depending on the crack length and the electrical path between the shells of the fiber. Figure 4e shows a simplified circuit model for the H_2-sensing mechanism. The PdNP/PU composite shells were aligned in a zigzag formation with a nonuniform crack length. There were N_i cracks of length d_i and electrical resistance R_c. Assuming that cracks having a length lower than the threshold value of d_T are closed when H_2 is introduced, the ratios of the closed cracks are as follows:

$$r = n/N = \frac{\sum_i N_i u(d_T - d_i)}{\sum_i N_i} \tag{2}$$

where $u(d_T - d_i)$ is a unit step function and N is the total number of cracks. Equation 2 can be rewritten using a normalized probability distribution of the crack length $p(x)$ as

$$r = \int_{-\infty}^{d_T} p(x)\mathrm{d}x \tag{3}$$

We can assume that $p(x)$ has a normal distribution with an average crack length of $d = d_0 + \delta\varepsilon$, where d_0 and δ are constants and ε is the applied strain. The standard deviation is σ. Equation 3 can then be calculated as

$$r = \frac{1}{2}\left(\mathrm{erfc}\left(\frac{d - d_T}{\sigma\sqrt{2}}\right)\right) \tag{4}$$

where $\mathrm{erfc}(x)$ is a complementary error function (see the Supporting Information).

The resistance of the repeating segment is R_{Air} in air and R_{H_2} in the H_2 environment. The total resistance after H_2 exposure is a parallel connection of R'_{Air} and n segments of R_C, where R'_{Air} is the resistance when R_{Air} is exposed to H_2, and can be written as

https://dx.doi.org/10.1021/acsami.0c10460
ACS Appl. Mater. Interfaces 2020, 12, 45243−45253

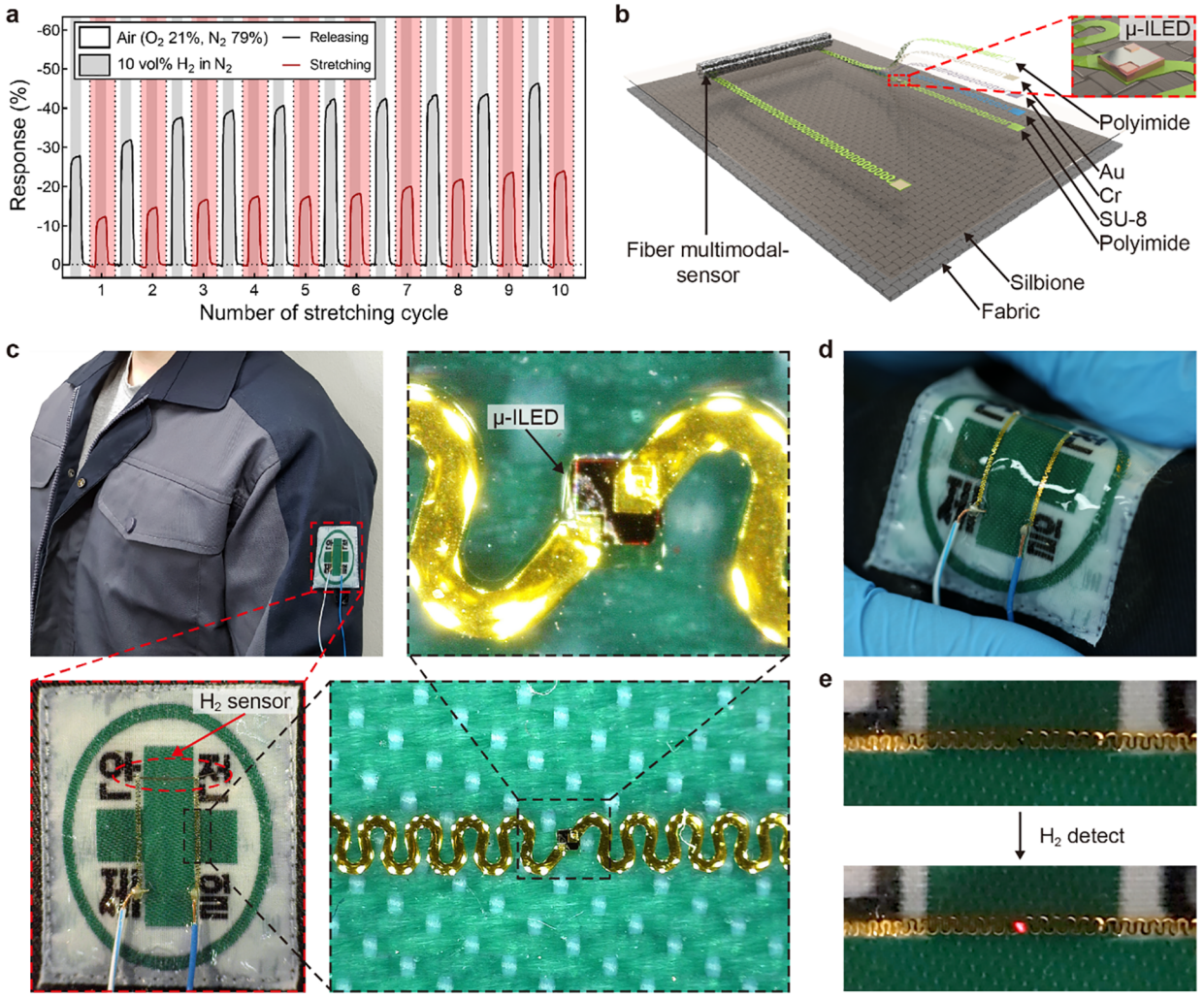

Figure 5. (a) Response of the fiber multimodal sensor when exposed to H_2 gas for 10 stretching−releasing cycles at 50% strain. (b) Schematic illustration and (c) real image of the fiber multimodal sensor connected to a μ-ILED on industrial safety clothing, reading "safety first." (d) Image showing the flexibility of the μ-ILED device. (e) Image of the μ-ILED when exposed to H_2 gas.

$$\frac{1}{R_{H_2}} = \frac{1}{R'_{Air}} + \frac{n}{R_C} = \frac{1}{R'_{Air}} + \frac{r}{R'_C} \tag{5}$$

where $R'_C = R_C/N$ is a constant. The theoretical response can be calculated from eqs 1, 4, and 5 as

$$\text{Response} = \frac{R'_C(R'_{Air}/R_{Air})}{R'_C + rR'_{Air}} - 1 \tag{6}$$

which well fits the experimental data shown in Figure 4g. A finite element method (FEM) simulation was also used to predict the behavior of the sensor under various applied strains. The PdNP/PU composite shells were modeled as two-dimensional plates connected in a zigzag shape using the parameters obtained from Figure 4c. The nonuniform crack was modeled using perpendicular cracks of different heights. The shells were then expanded to model the PdNP/PU composite expansion under H_2 exposure. Figure 4f shows the FEM results for the strain-free fiber and for the 20% strained fiber in air and H_2 environments. The arrows show the direction of the electrical current, and the size is proportional to the current density. Most of the current flows along the shell. However, under an H_2 environment of low strains, some of the small cracks can be connected, leading to the current flowing over the crack. By using the geometrical effect obtained from the FEM simulation, the results are fitted in Figure 4g, showing the agreement of tendency with the experimental values. The FEM results show a much steeper curve because we used a finite number of cracks for the model. Above 70% strain, the response of the fiber showed a different tendency that slightly increased. At a low strain range, fewer cracks and the electrical paths were formed in the air. Thus, as the strain increased, the H_2 gas response decreased due to disconnected Pd shells. At a high strain range, however, the volume expansion of the Pd shells due to the reaction with H_2 has more effect on conductivity. Thus, few electrical paths with high strain caused a large resistance change in the fiber exposed to H_2 gas. This induced an increase in response (Figure 4h,i). Figure 4j shows that the response decreased up to 70% strain and then increased over more strain until 110%.

Crack Effect upon Strain Application. When the applied strain was released, interesting findings were observed. Figure 5a shows the H_2 gas response of a newly fabricated fiber for 10 stretching−releasing cycles at 50% strain. The electrical resistance of the fiber in air increased because of the repeated straining. Additionally, the H_2 response of the strain-free-fiber increased after repeated stretching−releasing cycles. The

https://dx.doi.org/10.1021/acsami.0c10460
ACS Appl. Mater. Interfaces 2020, 12, 45243−45253

results show that the response of the H_2 gas sensitive fiber did not degrade but rather enhanced under repeated strain fatigue. The fiber-type sensor showed good durability against repeated H_2 exposure and strain, which makes it suitable for wearable H_2 gas detection. Initially, the sensing performance of the sensor may appear unstable as the stretching/releasing motions change the sensitivity of the sensor. However, this phenomenon could be solved through continuous stretching cycles. This can be explained by the crack structure and electrical paths that are formed within the initial and strain-damaged samples. Initially, the number of cracks in the fiber was limited. When the fiber was repeatedly strained, the number of cracks increased, ultimately leading to an increase in the electrical resistance and response size. The more and more cracks formed by repeatedly strain-damaging increased both the basic resistance in air (~100 MΩ) and the resistance in H_2 (~500 kΩ). At the same time, the amount of change in the resistance was also very large. Therefore, the H_2 sensitivity of the sensor could be improved because the more the cracks, the lower the H_2 responded resistance compared to the basic resistance in air. Similar results were previously observed by stretching Pd thin films on PDMS. However, the PU/PdNP composite cracks showed smaller, more random, and more irregular structures compared with the Pd film, enabling H_2 gas detection under strain application and making its properties easier to tune according to the level of the strain applied. We intend to demonstrate the performance of the fiber sensor highly damaged by repeated stretching through the following application.

Use of Stretchable H_2 Gas Sensors in Wearable Applications. We used the high response of the highly damaged fiber for the visualization of H_2 gas detection. Figure 5b,c shows a schematic and the real image of the fiber multimodal sensor connected to a μ-ILED integrated into industrial safety clothing for H_2 gas leakage warnings. We chose the highly damaged fiber having high response for this specific test. The fiber was connected to a μ-ILED via serpentine-shaped electrodes to reduce damage from the external mechanical stimulation.[52] Figure 5d and Movie S2 show that the device is stable under both bending and torsion, making it suitable for wearable applications. Figure 5e shows the image of the μ-ILED before and after H_2 exposure. Prior to exposure, the μ-ILED was off, and only 10 nA current was detected. When exposed to H_2 gas, the current gradually increases to 70 μA and the μ-ILED turned on after a few second delay (Figure S6 and Movie S3). The μ-ILED could be turned on and off by detecting H_2 gas exposure under external strain on the fiber for several cycles. Additionally, the activation of μ-ILED can be enhanced by using repeatedly strained fiber, which exhibits a large change in the resistance. As expected, it was confirmed that the fiber multimodal sensor connected to clothes showed an appropriate performance compared with those of the commercial H_2 gas sensors (Movie S4).

CONCLUSIONS

In summary, we developed a fiber multimodal sensor comprising a conductive PdNP/PU composite shell. The fiber sensor was successfully prepared by incorporating PdNPs in the outer shell of the PU fiber via a simple solution process. The developed sensor showed −27.3% response at 10% H_2 and −0.75% response at 5 ppm H_2 while maintaining the H_2 gas response at applied strains up to 110%. The change in the resistance of the fiber in H_2 gas was affected by two factors: the PdNP/PU composite effect and geometrical effect. The experimental results were in agreement with the theoretical and FEM simulation results. Repeated straining−releasing cycles revealed that the response size increased because of the newly generated cracks. Under the repeated strained case, the fiber lost its conductivity in air and recovered its conductivity when exposed to H_2 gas. In addition, the fiber multimodal sensor was converted into a functional wearable H_2 gas detector in clothing, having a connecting μ-ILED for visual alerting. We believe that this research provides the potential for future advancements in wearable sensors and textile electronics.

METHODS

Fabrication of the Fiber-Type Stretchable Multimodal Sensor. PU fiber (Taekwang Industrial Co. Ltd.) was used to produce resistive fibers. Pd trifluoroacetate ($Pd(CF_3COO)_2$, 97%, Alfa Aesar) (20 wt %) was dissolved in IPA (99.5%, Duksan Pure Chemicals). The polymer fiber was immersed in the precursor solution for 30 min and dried in open air for 10 min on a poly(tetrafluoroethylene) (PTFE) dish. Several droplets of 50% hydrazine hydrate ($N_2H_4{\cdot}xH_2O$, N_2H_4 50 ~ 60%, Sigma Aldrich) diluted in ethanol (99.9%, Duksan Pure Chemicals) were added onto the fiber for 10 min to chemically reduce Pd ions. The sample was then rinsed with deionized water and dried in open air.

Fabrication and Test of the μ-ILED Device. A glass slide (50 × 35 × 1 mm^3) was coated with poly(methyl methacrylate) (PMMA, MicroChem, USA), which served as a sacrificial layer to facilitate coating other films. Spin casting and thermal curing (2 h at 250 °C in a vacuum oven) of a polyimide film (HD Microsystems, USA; thickness: 2 μm) yielded an overcoat on the PMMA. The μ-ILED (300 × 300 × 2 μm^3; lab-built from an AlInGaP epitaxial wafer) was transfer printed onto a glass substrate coated with layers of a photocurable epoxy (SU-82002; MicroChem, USA; thickness: 2 μm) from μ-ILED arrays using a PDMS stamp (Sylgard 184; Dow Corning, USA) and a mask aligner (MDA-400S; MIDAS SYSTEM, Korea). Negative photoresist (SU-82002; MicroChem; thickness: 2 μm) was spin coated to define the electrical contact area pattern for μ-ILED electrodes. The bilayers of Cr (7 nm)/Au (200 nm), formed by electron beam evaporation and patterned by photolithography, were metal-etched to create the interconnections of the device and electrical lead-out. A final layer of the spin-cast negative photoresist (SU-82002; MicroChem; thickness: 2 μm) was passivated isolating the devices. Next, multiple polymer layers (epoxy-epoxy-PMMA) were etched from regions not protected by the masking layer via reactive ion etching (100 mTorr, 20 sccm O_2, and 150 W for 20−30 min). The PMMA layer was undercut to allow the release for subsequent integration with the fabric coated with a sticky elastomer (Silbione RT Gel 4717 A/B; Bluestar Silicone, France).

Characterization. The surface morphologies were examined using a JEOL JSM-7001F field-emission scanning electron microscope (FE-SEM) equipped with an EDS. FTIR results were obtained using a Bruker Vertex 70 in the attenuated total reflectance (ATR) mode. XRD results were obtained from a Rigaku SmartLab equipped with a Cu target X-ray tube. TGA results were obtained using a TA Instrument Q50 at 20 °C/min in N_2 gas. All electrical measurements were performed using a Kiethley 2400 source meter. Initial fiber lengths were fixed by placing the fibers on copper tapes having 2 cm gaps. The stretching experiment was carried out using a custom-made stretching machine (Figure S8). The samples were measured inside a quartz tube chamber while diluted H_2 gas (100 ppm, 0.5 and 10% in N_2), N_2, and air (79% N_2 and 21% O_2) were inserted inside the chamber with programmed ratios using mass flow controllers. FEM simulation was conducted using COMSOL 5.0.

https://dx.doi.org/10.1021/acsami.0c10460
ACS Appl. Mater. Interfaces 2020, 12, 45243−45253

■ ASSOCIATED CONTENT

Supporting Information

The Supporting Information is available free of charge at https://pubs.acs.org/doi/10.1021/acsami.0c10460.

Stretchability of the H_2-sensitive conductive fiber (MP4)

Flexibility of the fabricated μ-ILED device (MP4)

Operation of the μ-ILED device under an H_2/air environment (MP4)

Operation of the μ-ILED device under an H_2/air environment with a commercial sensor (MP4)

Theoretical calculations related to the H_2 gas-sensing property of the PdNP/PU composite; theoretical model calculation of H_2 gas sensing under strain; HSP calculation of PU, methanol, and isopropyl alcohol; image of the as-received fiber and after reduction; XRD patterns of the fiber; TGA results of the fiber; SEM image of the methanol-based sample; gas-sensing characteristics of the methanol-based sample; μ-ILED characteristics and current when connected to the fiber H_2 gas sensor; and illustration of case II diffusion (PDF)

■ AUTHOR INFORMATION

Corresponding Authors

Yongfeng Mei − *School of Electrical and Electronic Engineering, Yonsei University, Seoul 03722, Republic of Korea; Department of Materials Science, Fudan University, Shanghai 200433, China;* orcid.org/0000-0002-3314-6108; Email: yfm@fudan.edu.cn

Kyung-In Jang − *Department of Robotics Engineering, Daegu Gyeongbuk Institute of Science and Technology, Daegu 42988, Republic of Korea*; Email: kijang@dgist.ac.kr

Taeyoon Lee − *School of Electrical and Electronic Engineering, Yonsei University, Seoul 03722, Republic of Korea; Center for BioMicrosystems, Brain Science Institute, Korea Institute of Science and Technology (KIST), Seoul 02792, Republic of Korea*; Email: taeyoon.lee@yonsei.ac.kr

Authors

Chihyeong Won − *School of Electrical and Electronic Engineering, Yonsei University, Seoul 03722, Republic of Korea*

Sanggeun Lee − *School of Electrical and Electronic Engineering, Yonsei University, Seoul 03722, Republic of Korea*

Han Hee Jung − *Department of Robotics Engineering, Daegu Gyeongbuk Institute of Science and Technology, Daegu 42988, Republic of Korea*

Janghoon Woo − *School of Electrical and Electronic Engineering, Yonsei University, Seoul 03722, Republic of Korea*

Kukro Yoon − *School of Electrical and Electronic Engineering, Yonsei University, Seoul 03722, Republic of Korea*

Jaehong Lee − *Department of Robotics Engineering, Daegu Gyeongbuk Institute of Science and Technology, Daegu 42988, Republic of Korea*

Chaebeen Kwon − *School of Electrical and Electronic Engineering, Yonsei University, Seoul 03722, Republic of Korea*

Minkyu Lee − *School of Electrical and Electronic Engineering, Yonsei University, Seoul 03722, Republic of Korea*

Heetak Han − *School of Electrical and Electronic Engineering, Yonsei University, Seoul 03722, Republic of Korea*

Complete contact information is available at: https://pubs.acs.org/10.1021/acsami.0c10460

Author Contributions

C.W. conducted the overall experiments, measurements, and analysis and wrote the manuscript. S.L. provided the assistance on the fabrication of the fiber and performed computational simulation for the crack process of the Pd rich shell. H.H.J. and K.-I.J. fabricated the light-emitting diode device on clothing. J.W., K.Y., J.L, C.K., and M.L. provided helpful discussions on data analysis. Y.M. and T.L. supervised the project.

Notes

The authors declare no competing financial interest.

■ ACKNOWLEDGMENTS

This research was supported by the National Research Foundation of Korea (NRF) funded by the Ministry of Science and ICT (NRF-2017M3A7B4049466, NRF-2019M3C1B8090845, and NRF-2017M3A9G8084463). This work was also supported by the Priority Research Centers Program through the NRF (NRF-2019R1A6A1A11055660). This work was supported by the KIST Institutional Program (Project No. 2Z06430-20-P064). This research was partially supported by the Graduate School of YONSEI University Research Scholarship Grants in 2018.

■ REFERENCES

(1) Zeng, W.; Shu, L.; Li, Q.; Chen, S.; Wang, F.; Tao, X.-M. Fiber-Based Wearable Electronics: A Review of Materials, Fabrication, Devices, and Applications. *Adv. Mater.* **2014**, *26*, 5310−5336.

(2) Weng, W.; Chen, P.; He, S.; Sun, X.; Peng, H. Smart Electronic Textiles. *Angew. Chem., Int. Ed.* **2016**, *55*, 6140−6169.

(3) Wang, L.; Fu, X.; He, J.; Shi, X.; Chen, T.; Chen, P.; Wang, B.; Peng, H. Application Challenges in Fiber and Textile Electronics. *Adv. Mater.* **2020**, *32*, 1901971.

(4) Sun, H.; Zhang, Y.; Zhang, J.; Sun, X.; Peng, H. Energy Harvesting and Storage in 1D Devices. *Nat. Rev. Mater.* **2017**, *2*, 17023.

(5) Zhu, Y.-H.; Yang, X.-Y.; Liu, T.; Zhang, X.-B. Flexible 1D Batteries: Recent Progress and Prospects. *Adv. Mater.* **2020**, *32*, 1901961.

(6) Lee, J.; Llerena Zambrano, B.; Woo, J.; Yoon, K.; Lee, T. Recent Advances in 1D Stretchable Electrodes and Devices for Textile and Wearable Electronics: Materials, Fabrications, and Applications. *Adv. Mater.* **2020**, *32*, 1902532.

(7) Janas, D.; Koziol, K. K. Carbon Nanotube Fibers and Films: Synthesis, Applications and Perspectives of the Direct-Spinning Method. *Nanoscale* **2016**, *8*, 19475−19490.

(8) Jang, Y.; Kim, S. M.; Spinks, G. M.; Kim, S. J. Carbon Nanotube Yarn for Fiber-Shaped Electrical Sensors, Actuators, and Energy Storage for Smart Systems. *Adv. Mater.* **2020**, *32*, 1902670.

(9) Xin, G.; Yao, T.; Sun, H.; Scott, S. M.; Shao, D.; Wang, G.; Lian, J. Highly Thermally Conductive and Mechanically Strong Graphene Fibers. *Science* **2015**, *349*, 1083.

(10) Yeo, C. S.; Kim, H.; Lim, T.; Kim, H. J.; Cho, S.; Cho, K. R.; Kim, Y. S.; Shin, M. K.; Yoo, J.; Ju, S.; Park, S. Y. Copper-Embedded Reduced Graphene Oxide Fibers for Multi-Sensors. *J. Mater. Chem. C* **2017**, *5*, 12825−12832.

(11) Zhang, Z.; Cui, L.; Shi, X.; Tian, X.; Wang, D.; Gu, C.; Chen, E.; Cheng, X.; Xu, Y.; Hu, Y.; Zhang, J.; Zhou, L.; Fong, H. H.; Ma, P.; Jiang, G.; Sun, X.; Zhang, B.; Peng, H. Textile Display for Electronic and Brain-Interfaced Communications. *Adv. Mater.* **2018**, *30*, 1800323.

(12) Zhao, X.; Chen, F.; Li, Y.; Lu, H.; Zhang, N.; Ma, M. Bioinspired Ultra-Stretchable and Anti-Freezing Conductive Hydrogel Fibers with Ordered and Reversible Polymer Chain Alignment. *Nat. Commun.* **2018**, *9*, 3579.

(13) Park, M.; Im, J.; Shin, M.; Min, Y.; Park, J.; Cho, H.; Park, S.; Shim, M. B.; Jeon, S.; Chung, D. Y.; Bae, J.; Park, J.; Jeong, U.; Kim,

K. Highly Stretchable Electric Circuits from a Composite Material of Silver Nanoparticles and Elastomeric Fibres. *Nat. Nanotechnol.* **2012**, *7*, 803.
(14) Lee, J.; Kwon, H.; Seo, J.; Shin, S.; Koo, J. H.; Pang, C.; Son, S.; Kim, J. H.; Jang, Y. H.; Kim, D. E.; Lee, T. Conductive Fiber-Based Ultrasensitive Textile Pressure Sensor for Wearable Electronics. *Adv. Mater.* **2015**, *27*, 2433−2439.
(15) Lee, S.; Shin, S.; Lee, S.; Seo, J.; Lee, J.; Son, S.; Cho, H. J.; Algadi, H.; Al-Sayari, S.; Kim, D. E.; Lee, T. Ag Nanowire Reinforced Highly Stretchable Conductive Fibers for Wearable Electronics. *Adv. Funct. Mater.* **2015**, *25*, 3114−3121.
(16) Choi, S.; Han, S. I.; Jung, D.; Hwang, H. J.; Lim, C.; Bae, S.; Park, O. K.; Tschabrunn, C. M.; Lee, M.; Bae, S. Y.; Yu, J. W.; Ryu, J. H.; Lee, S.-W.; Park, K.; Kang, P. M.; Lee, W. B.; Nezafat, R.; Hyeon, T.; Kim, D.-H. Highly Conductive, Stretchable and Biocompatible Ag−Au Core−Sheath Nanowire Composite for Wearable and Implantable Bioelectronics. *Nat. Nanotechnol.* **2018**, *13*, 1048−1056.
(17) Klinkova, A.; De Luna, P.; Dinh, C.-T.; Voznyy, O.; Larin, E. M.; Kumacheva, E.; Sargent, E. H. Rational Design of Efficient Palladium Catalysts for Electroreduction of Carbon Dioxide to Formate. *ACS Catal.* **2016**, *6*, 8115−8120.
(18) Rao, R. G.; Blume, R.; Hansen, T. W.; Fuentes, E.; Dreyer, K.; Moldovan, S.; Ersen, O.; Hibbitts, D. D.; Chabal, Y. J.; Schlögl, R.; Tessonnier, J.-P. Interfacial Charge Distributions in Carbon-Supported Palladium Catalysts. *Nat. Commun.* **2017**, *8*, 340.
(19) Wang, F.; Zhang, Y.; Du, Z.; Ren, J.; Qu, X. Designed Heterogeneous Palladium Catalysts for Reversible Light-Controlled Bioorthogonal Catalysis in Living Cells. *Nat. Commun.* **2018**, *9*, 1209.
(20) Kishore, S.; Nelson, J. A.; Adair, J. H.; Eklund, P. C. Hydrogen Storage in Spherical and Platelet Palladium Nanoparticles. *J. Alloys Compd.* **2005**, *389*, 234−242.
(21) Li, G.; Kobayashi, H.; Taylor, J. M.; Ikeda, R.; Kubota, Y.; Kato, K.; Takata, M.; Yamamoto, T.; Toh, S.; Matsumura, S.; Kitagawa, H. Hydrogen Storage in Pd Nanocrystals Covered with a Metal−Organic Framework. *Nat. Mater.* **2014**, *13*, 802−806.
(22) Dekura, S.; Kobayashi, H.; Kusada, K.; Kitagawa, H. Hydrogen in Palladium and Storage Properties of Related Nanomaterials: Size, Shape, Alloying, and Metal-Organic Framework Coating Effects. *ChemPhysChem* **2019**, *20*, 1158−1176.
(23) Favier, F.; Walter, E. C.; Zach, M. P.; Benter, T.; Penner, R. M. Hydrogen Sensors and Switches from Electrodeposited Palladium Mesowire Arrays. *Science* **2001**, *293*, 2227.
(24) Im, Y.; Lee, C.; Vasquez, R. P.; Bangar, M. A.; Myung, N. V.; Menke, E. J.; Penner, R. M.; Yun, M. Investigation of a Single Pd Nanowire for Use as a Hydrogen Sensor. *Small* **2006**, *2*, 356−358.
(25) Yang, F.; Taggart, D. K.; Penner, R. M. Joule Heating a Palladium Nanowire Sensor for Accelerated Response and Recovery to Hydrogen Gas. *Small* **2010**, *6*, 1422−1429.
(26) Zeng, X. Q.; Latimer, M. L.; Xiao, Z. L.; Panuganti, S.; Welp, U.; Kwok, W. K.; Xu, T. Hydrogen Gas Sensing with Networks of Ultrasmall Palladium Nanowires Formed on Filtration Membranes. *Nano Lett.* **2011**, *11*, 262−268.
(27) Hong, J.; Lee, S.; Seo, J.; Pyo, S.; Kim, J.; Lee, T. A Highly Sensitive Hydrogen Sensor with Gas Selectivity Using a PMMA Membrane-Coated Pd Nanoparticle/Single-Layer Graphene Hybrid. *ACS Appl. Mater. Interfaces* **2015**, *7*, 3554−3561.
(28) Zhang, J.; Liu, X.; Neri, G.; Pinna, N. Nanostructured Materials for Room-Temperature Gas Sensors. *Adv. Mater.* **2016**, *28*, 795−831.
(29) Jang, J. S.; Qiao, S.; Choi, S. J.; Jha, G.; Ogata, A. F.; Koo, W. T.; Kim, D. H.; Kim, I. D.; Penner, R. M. Hollow Pd-Ag Composite Nanowires for Fast Responding and Transparent Hydrogen Sensors. *ACS Appl. Mater. Interfaces* **2017**, *9*, 39464−39474.
(30) Vogel, W.; He, W.; Huang, Q. H.; Zou, Z.; Zhang, X. G.; Yang, H. Palladium Nanoparticles "Breathe" Hydrogen; a Surgical View with X-Ray Diffraction. *Int. J. Hydrogen Energy* **2010**, *35*, 8609−8620.
(31) Smith, R. J.; Otterson, D. A. Electrical Resistivity of PdHx System for H Pd Atom Ratios to 0·97. *J. Phys. Chem. Solids* **1970**, *31*, 187−189.
(32) Lee, J.; Shim, W.; Lee, E.; Noh, J.-S.; Lee, W. Highly Mobile Palladium Thin Films on an Elastomeric Substrate: Nanogap-Based Hydrogen Gas Sensors. *Angew. Chem. Int. Ed.* **2011**, *50*, 5301−5305.
(33) Kim, S.; Lee, H.-S.; Jang, B.; Cho, S.; Lee, W. Strain-Controlled Nanocrack Formation in a Pd Film on Polydimethylsiloxane for the Detection of Low H2 Concentrations. *J. Mater. Sci.* **2016**, *51*, 4530−4537.
(34) Jang, J.-S.; Qiao, S.; Choi, S.-J.; Jha, G.; Ogata, A. F.; Koo, W.-T.; Kim, D.-H.; Kim, I.-D.; Penner, R. M. Hollow Pd−Ag Composite Nanowires for Fast Responding and Transparent Hydrogen Sensors. *ACS Appl. Mater. Interfaces* **2017**, *9*, 39464−39474.
(35) Xie, B.; Mao, P.; Chen, M.; Li, Z.; Han, J.; Yang, L.; Wang, X.; Han, M.; Liu, J.-M.; Wang, G. Pd Nanoparticle Film on a Polymer Substrate for Transparent and Flexible Hydrogen Sensors. *ACS Appl. Mater. Interfaces* **2018**, *10*, 44603−44613.
(36) Namgung, G.; Ta, Q. T. H.; Noh, J.-S. Stretchable Hydrogen Sensors Employing Palladium Nanosheets Transferred onto an Elastomeric Substrate. *Chem. Phys. Lett.* **2018**, *703*, 86−93.
(37) Kim, D.-H.; Kim, S.-J.; Shin, H.; Koo, W.-T.; Jang, J.-S.; Kang, J.-Y.; Jeong, Y. J.; Kim, I.-D. High-Resolution, Fast, and Shape-Conformable Hydrogen Sensor Platform: Polymer Nanofiber Yarn Coupled with Nanograined Pd@Pt. *ACS Nano* **2019**, *13*, 6071−6082.
(38) Gong, S.; Yap, L. W.; Zhu, B.; Zhai, Q.; Liu, Y.; Lyu, Q.; Wang, K.; Yang, M.; Ling, Y.; Lai, D. T. H.; Marzbanrad, F.; Cheng, W. Local Crack-Programmed Gold Nanowire Electronic Skin Tattoos for In-Plane Multisensor Integration. *Adv. Mater.* **2019**, *31*, 1903789.
(39) Gong, S.; Yap, L. W.; Zhu, Y.; Zhu, B.; Wang, Y.; Ling, Y.; Zhao, Y.; An, T.; Lu, Y.; Cheng, W. A Soft Resistive Acoustic Sensor Based on Suspended Standing Nanowire Membranes with Point Crack Design. *Adv. Funct. Mater.* **2020**, *30*, 1910717.
(40) Lee, J.; Shin, S.; Lee, S.; Song, J.; Kang, S.; Han, H.; Kim, S.; Kim, S.; Seo, J.; Kim, D.; Lee, T. Highly Sensitive Multifilament Fiber Strain Sensors with Ultrabroad Sensing Range for Textile Electronics. *ACS Nano* **2018**, *12*, 4259−4268.
(41) Hansen, C. M. *Hansen Solubility Parameters, Introduction - A User's Handbook*. CRC Press, 2007.
(42) Crank, J. *The Mathematics of Diffusion*, Second Edition. Oxford Univ. Press, 1975.
(43) Seyedin, S.; Zhang, P.; Naebe, M.; Qin, S.; Chen, J.; Wang, X.; Razal, J. M. Textile Strain Sensors: A Review of the Fabrication Technologies, Performance Evaluation and Applications. *Mater. Horizons* **2019**, *6*, 219−249.
(44) Shin, D. H.; Lee, J. S.; Jun, J.; An, J. H.; Kim, S. G.; Cho, K. H.; Jang, J. Flower-like Palladium Nanoclusters Decorated Graphene Electrodes for Ultrasensitive and Flexible Hydrogen Gas Sensing. *Sci. Rep.* **2015**, *5*, 12294.
(45) Karim, G. A. Hydrogen as a Spark Ignition Engine Fuel. *Int. J. Hydrogen Energy* **2002**, *28*, 569−577.
(46) Han, H.; Baik, S.; Xu, B.; Seo, J.; Lee, S.; Shin, S.; Lee, J.; Koo, J. H.; Mei, Y.; Pang, C.; Lee, T. Bioinspired Geometry-Switchable Janus Nanofibers for Eye-Readable H2Sensors. *Adv. Funct. Mater.* **2017**, *27*, 1701618.
(47) Vogel, W.; He, W.; Huang, Q.-H.; Zou, Z.; Zhang, X.-G.; Yang, H. Palladium Nanoparticles "Breathe" Hydrogen; a Surgical View with X-Ray Diffraction. *Int. J. Hydrogen Energy* **2010**, *35*, 8609−8620.
(48) Noh, J. S.; Kim, H.; Kim, B. S.; Lee, E.; Cho, H. H.; Lee, W. High-Performance Vertical Hydrogen Sensors Using Pd-Coated Rough Si Nanowires. *J. Mater. Chem.* **2011**, *21*, 15935.
(49) Xu, T.; Zach, M. P.; Xiao, Z. L.; Rosenmann, D.; Welp, U.; Kwok, W. K.; Crabtree, G. W. Self-Assembled Monolayer-Enhanced Hydrogen Sensing with Ultrathin Palladium Films. *Appl. Phys. Lett.* **2005**, *86*, 1−3.
(50) Lee, J.; Noh, J. S.; Lee, S. H.; Song, B.; Jung, H.; Kim, W.; Lee, W. Cracked Palladium Films on an Elastomeric Substrate for Use as Hydrogen Sensors. *Int. J. Hydrogen Energy* **2012**, *37*, 7934−7939.
(51) Kang, D.; Pikhitsa, P. V.; Choi, Y. W.; Lee, C.; Shin, S. S.; Piao, L.; Park, B.; Suh, K. Y.; Kim, T. I.; Choi, M. Ultrasensitive Mechanical Crack-Based Sensor Inspired by the Spider Sensory System. *Nature* **2014**, *516*, 222−226.

https://dx.doi.org/10.1021/acsami.0c10460
ACS Appl. Mater. Interfaces 2020, 12, 45243−45253

(52) Kim, D.-H.; Lu, N.; Ma, R.; Kim, Y.-S.; Kim, R.-H.; Wang, S.; Wu, J.; Won, S. M.; Tao, H.; Islam, A.; Yu, K. J.; Kim, T.; Chowdhury, R.; Ying, M.; Xu, L.; Li, M.; Chung, H.-J.; Keum, H.; McCormick, M.; Liu, P.; Zhang, Y.-W.; Omenetto, F. G.; Huang, Y.; Coleman, T.; Rogers, J. A. Epidermal Electronics. *Science* **2011**, *333*, 838−843.

https://dx.doi.org/10.1021/acsami.0c10460
ACS Appl. Mater. Interfaces 2020, 12, 45243−45253